Thermohydraulic performance evaluation of internally finned elliptical geothermal collector pipes

Niklas Hidman[1]

[1]Division of Fluid Dynamics, Department of Mechanical and Maritime Sciences, Chalmers University of Technology, Gothenburg, Sweden

June 8, 2026

1 Introduction

In this report we evaluate, using fully resolved Direct Numerical Simulations (DNS), the thermohydraulic performance of smooth and internally finned (alternating helical fins) elliptical pipes. The target application is collector pipes in geothermal systems, but the results are applicable to other heat exchanger pipes under similar operating conditions. The methodology and results are compared to those for circular pipes reported in Hidman *et al.* (2026).

Elliptical collector pipes represent a promising alternative to conventional circular pipes for two practical reasons. First, an elliptical cross-section can fit into a narrower borehole than a circular pipe of the same cross-sectional area, potentially reducing drilling costs. Second, the larger semi-major axis of the ellipse more closely matches the borehole wall radius, placing the pipe wall in closer proximity to the borehole wall and thereby reducing the thermal resistance between the pipe and the surrounding ground.

The key design requirements for geothermal collector pipes are the same as identified in Hidman *et al.* (2026): the fins should promote the transition to an unsteady flow at $Re < Re_c \approx 2300$ (where the convective resistance constitutes roughly 50% of the total borehole thermal resistance and where enhanced heat transfer thus gives the largest system-level benefit) without significantly increasing the friction factor at $Re > Re_c$, where excessive pressure drop may reduce the net efficiency of the system. The present study evaluates whether these objectives can be met for elliptical pipe geometries, and how the thermohydraulic performance of smooth and finned elliptical pipes compares to the corresponding circular pipe results of Hidman *et al.* (2026) and to standard correlations for smooth circular pipes.

2 Methodology

Collector pipes are generally several hundreds of meters long, so entrance region effects can be neglected and we focus on evaluating the thermohydraulic performance at fully developed conditions, limited to the convective heat transfer between the pipe inner wall and the liquid; for further details on the numerical framework, see Hidman *et al.* (2026).

For the elliptical pipe geometry, the pipe diameter D in the definitions of Re and Nu is replaced by the hydraulic diameter $D_h = 4A/P$, where A is the cross-sectional area and P is the wetted perimeter

of the ellipse.

2.1 Numerical framework

We study, using Direct Numerical Simulations (DNS), fully developed flow in elliptical pipes, with and without surface modifications (fins), using periodic boundary conditions in the axial x-direction. The pipe in the computational domain has semi-major axis a, semi-minor axis b, hydraulic diameter $D_h = 4A/P$ and length L. The cross-sectional area and wetted perimeter of the ellipse are given by

$$A = \pi a b \,, \tag{1}$$

$$P = 4a \int_0^{\pi/2} \sqrt{1 - e^2 \sin^2\theta}\, d\theta \,, \tag{2}$$

where $e = \sqrt{1-(b/a)^2}$ is the eccentricity of the ellipse. The wall boundary conditions are no slip $\boldsymbol{u} = 0$ and constant wall temperature $T_w > T_b$ where the bulk temperature is defined as $T_b = \dfrac{1}{\Omega_l}\int_{\Omega_l} Tu\, d\Omega$, the Ω_l is the liquid volume and u is the axial velocity component. The temperature is assumed a passive scalar since typical temperature variations in geothermal collector systems is only about 5°C. All material properties are thus assumed constant. This simplification also allows us to evolve several temperature fields in the same simulation case.

In the remainder of this report (unless otherwise stated), all variables are made non-dimensional by the hydraulic diameter D_h, bulk velocity $U_b = \dfrac{1}{\Omega_l}\int_{\Omega_l} u\, d\Omega$ and liquid density ρ: $x_i^* = x_i/D_h$, $u_i^* = u_i/U_b$, $t^* = tU_b/D_h$, $p^* = p/(\rho U_b^2)$. The non-dimensional temperature is defined as $T^* = (T - T_b)/(T_w - T_b)$ that gives a $T_w^* = 1$ and $T_b^* = 0$. The asterisk notation is hereafter omitted for brevity. The non-dimensional governing equations then becomes

$$\nabla \cdot \boldsymbol{u} = 0 \,, \tag{3}$$

$$\frac{\partial \boldsymbol{u}}{\partial t} + (\boldsymbol{u}\cdot\nabla)\boldsymbol{u} = -\nabla p + \frac{1}{Re}\nabla\cdot(2\mu \boldsymbol{S}) + \boldsymbol{a} \,, \tag{4}$$

$$\frac{\partial T}{\partial t} + \boldsymbol{u}\cdot\nabla T = \frac{1}{RePr}\nabla^2 T + S_Q \,, \tag{5}$$

where $\boldsymbol{u}$ is the velocity, p the pressure, $\boldsymbol{S} = (\nabla\boldsymbol{u} + \nabla\boldsymbol{u}^T)/2$ the rate of deformation tensor, $\boldsymbol{a}$ is the uniform axial driving force required to maintain a constant axial flow rate, T is the liquid temperature and S_Q is the uniform cooling term required to maintain a constant bulk temperature and thus axial periodicity of the temperature field. The present problem then becomes completely described by specifying the Reynolds $Re = U_b D_h/\nu$ and Prandtl $Pr = c_p\mu/k$ numbers (where c_p is the specific heat and k is the thermal conductivity). We investigate the parameter ranges of $1300 \leq Re \leq 3300$ and $20 \leq Pr \leq 75$ that are relevant for geothermal collector systems. It is also in this range of Re-numbers that we expect the transition from laminar to unsteady flow.

The governing equations are solved using the open-source code Basilisk (`basilisk.fr`) where the geometry is parametrised and defined using the embedded boundary method and constructive solid geometry operations. The non-dimensional bulk velocity $U_b = 1$ is forced by applying a time-dependent but spatially uniform acceleration term a_x in (4) (determined using a PI-controller). At steady flow conditions, the total forcing $F_a = \Omega_l \rho a_x$ equals the equivalent steady pressure drop over the pipe $F_p = A\Delta p$ that gives $\Delta p/L = \rho a_x$ (assuming the total liquid volume $\Omega_l = AL$ is approximately correct even with surface modifications). Defining the pipe friction factor f as $\Delta p = f(L/D_h)(\rho U_b^2/2)$ then gives $f = 2a_x D_h/U_b^2$.

The same methodology is used in the energy equation (5) where S_Q is varied uniformly (with another PI-controller) to force $T_b = 0$, similarly to the methodology of Pirozzoli *et al.* (2022). At statistically steady conditions, the total cooling rate $Q_c = \Omega_l S_Q$ equals the total wall heat flux $Q_w = q_w PL$. The wall heat flux is thus $q_w = S_Q A/P = S_Q D_h/4$. With the convective heat transfer coefficient $h = q_w/(T_w - T_b)$ we further define the non-dimensional Nusselt-number as $Nu = hD_h/k$ that represents the ratio of convective to conductive heat transfer rate.

For a fully developed laminar flow with $U_b = 1$ in smooth circular pipes of radius $R = D/2$, the axial velocity profile is $u(r) = 2(1 - (r/R)^2)$, where r is the radial coordinate from the pipe centre. With the uniform cooling term S_Q, the temperature profile is constant in the axial direction and the energy equation in polar coordinates reduces to

$$\frac{1}{RePr}\frac{1}{r}\frac{\partial}{\partial r}\left(r\frac{\partial T}{\partial r}\right) = -S_Q\,. \tag{6}$$

The radial temperature profile $T(r) = RePr\dfrac{S_Q}{4}(R^2 - r^2) + 1$ can then be obtained by integrating twice and applying the boundary conditions $T(R)$=1 and $\partial T/\partial r(r$=0)=0. By further imposing $T_b = \dfrac{1}{\pi R^2}\int_0^R Tu2\pi r dr = 0$, we can solve for $S_Q = -6/(R^2 RePr)$. The latter result gives a theoretical $Nu_{smooth,lam} = 6$ for laminar flow in smooth pipes with our numerical approach. This is thus the lower limit of Nu-numbers that we should expect from the simulations. For smooth elliptical pipes, no analogous closed-form solution exists; however, our DNS results confirm that $Nu \approx 6$ also for the elliptical geometry eveluated here at the lowest Re where the flow is laminar.

It should be noted that $Nu_{smooth,lam} = 6$ deviates from the classical result $Nu \approx 3.66$ valid for smooth pipes with laminar flow and a constant wall temperature without any cooling term. In the latter case, the bulk temperature asymptotically approaches the wall temperature along the axial direction of the pipe and it would not be possible to use a periodic axial boundary condition. Because of the high computational cost of DNS, the use of a relatively short periodic domain is necessary. Nevertheless, our approach gives heat transfer rates that remain suitable for relative comparison but are also close to experimental correlations and cases without the cooling term in the unsteady flow regime (Pirozzoli *et al.*, 2022).

The transition to turbulence for a smooth pipe typically occurs at about $Re_c = 2300$ but the exact value may vary in the range of $2000 \lessapprox Re \lessapprox 4000$ depending on inlet/initial conditions, the wall roughness or other flow disturbances. Since Re is here defined using D_h, the transition to turbulence for the smooth elliptical pipe is expected to occur at approximately the same $Re_c \approx 2300$ as for a smooth circular pipe (Hidman *et al.*, 2026). In real geothermal collector systems we anticipate significant disturbances by the recirculation pump, wall defects, pipe bends etc. To mimic these conditions, we simulate all designs first at a Reynolds number of $Re = 3300$ or $Re = 2300$ where the flow always becomes turbulent. Then, we successively lower the Re-number in the discrete steps of $Re = (3300, 2300, 2050, 1950, 1850, 1800, 1700, 1300)$. For each reduction, we let the flow reach a statistically steady (fully developed) condition before we reduce the Re-number further. This approach ensures that the initial conditions for a specific geometry and Re-number is always a relevant unsteady flow solution until a laminar solution is reached (all velocity fluctuations are dampened). The results (typically Nu and f) from each geometry and Re-number case are time-averaged during the fully developed conditions until the values are practically independent of the averaging period.

2.2 Grid study and validation

The numerical grid and its validation for smooth circular pipes are described in detail in Hidman *et al.* (2026). We adopt the same base grid here, consisting of cubic cells with side length $\Delta = D_h/58$ in

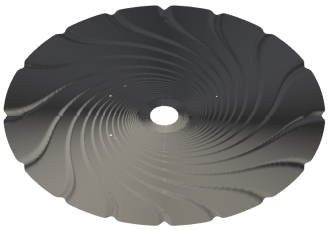

(a)

(b)

Figure 1: Illustration of the elliptical pipe geometry with alternating helical fins ($n_{fin} = 16$, $h_{fin} = 0.6$ mm, $\omega_{fin} = 360°$). (a): Cross-sectional view showing the internal fin arrangement. (b): Axial view of the pipe over one full period $L = 35D_h$.

the pipe core and a refinement region of approximately 10 cells at the wall with $\Delta = D_h/116$, giving $y^+ \approx 1$ for the cell closest to the wall. For the most challenging case ($Re = 3300$, $Pr = 75$), the relative error of the base grid is estimated to be about 5% or less, which is deemed sufficient for the present study. In addition, we validate our DNS results for smooth elliptical pipes against available experimental and analytical correlations for friction factor and heat transfer, as presented in section 3.

3 Results

We evaluate the thermohydraulic performance of smooth and finned elliptical pipes, where the fin design (alternating helical fins with the promising parameters identified in Hidman *et al.* (2026)) is applied directly without further parameter optimisation. We start by validating the smooth elliptical pipe results against available correlations, and then compare the thermohydraulic performance of the smooth and finned elliptical pipes in section 3.1. Next, we compare the regression models for the friction factor and heat transfer of the finned elliptical and finned circular pipes in section 3.2. Finally, we compare the performance of the finned elliptical and finned circular pipes at the same volumetric flow rate Q in section 3.2.1.

3.1 Smooth and finned elliptical pipes

Here, we compare the thermohydraulic performance of smooth and finned elliptical pipes, where the fin design follows the promising alternating helical configuration identified in Hidman *et al.* (2026), illustrated in figure 1, with $L = 35D_h$, $h_{fin} = 0.015D_h$, $n_{fin} = 16$ and $\omega_{fin} = 360°$. The elliptical cross-section has semi-major and semi-minor axes $a/D_h = 0.62$ and $b/D_h = 0.425$, respectively. The smooth elliptical pipe domain has length $L = 8.8D_h$. We evaluate three different $Pr = (20, 40, 75)$ at the operating conditions $Re = (3300, 2300, 2050, 1950, 1850, 1800, 1700, 1300)$, and compare the results to available correlations for smooth circular pipes and to the circular pipe DNS results of Hidman *et al.* (2026).

Figure 2 shows the friction factor for the smooth and finned elliptical pipes together with the laminar solution $f_{laminar}^{ellipse} = 65/Re$, the regression model for the finned elliptical pipe $f_{reg}^{ellipse,alternating}$ and the

correlation by Haaland (1983) (±5%). The smooth elliptical pipe shows excellent agreement with the laminar solution at $Re < 2300$ and with the Haaland correlation at $Re \geq 2300$, validating our numerical approach. For the finned elliptical pipe, a transition to an unsteady flow is observed at about $1850 < Re < 1950$, slightly higher than the circular pipe results of Hidman *et al.* (2026). Outside of this intermediate region, the friction factor of the finned elliptical pipe is practically the same as that of the smooth elliptical pipe, and both are in good agreement with the Haaland correlation at $Re \geq 2300$.

The laminar friction factor for an elliptical pipe, $f_{laminar}^{ellipse} = 65/Re$, is obtained from the analytical solution for fully developed laminar flow in an elliptical duct (White & Majdalani, 2006), where the constant 65 (compared to 64 for a circular pipe) reflects the increased viscous resistance due to the elliptical cross-section with $a/D_h = 0.62$ and $b/D_h = 0.425$.

The regression models for the friction factor of the finned elliptical and finned circular pipes are given by

$$f_{reg}^{ellipse,alternating} = (1 - s_e)\,\frac{65}{Re} + s_e \left(-1.8 \log_{10} \frac{6.9}{Re}\right)^{-2}, \tag{7}$$

$$f_{reg}^{circ,alternating} = (1 - s_c)\,\frac{64}{Re} + s_c \left(-1.8 \log_{10} \frac{6.9}{Re}\right)^{-2}, \tag{8}$$

where the sigmoid blending functions are

$$s_e = \left(1 + \exp\left(-\frac{5(Re - 1850)}{2300 - 1850} + 2.5\right)\right)^{-1}, \tag{9}$$

$$s_c = \left(1 + \exp\left(-\frac{5(Re - 1700)}{2300 - 1700} + 2.5\right)\right)^{-1}. \tag{10}$$

Both models blend smoothly between the laminar solution and the correlation by Haaland (1983) for turbulent flow, with the transition beginning at $Re = 1850$ for the elliptical pipe and $Re = 1700$ for the circular pipe, reflecting the slightly higher transition Reynolds number observed for the elliptical geometry.

Figure 3(a) shows the *Nu*-numbers for the smooth elliptical pipe together with the Meyer correlation (Meyer *et al.*, 2019) (±10%) and the laminar solution $Nu_{lam} = 6$. The DNS results are in fair agreement with the Meyer correlation at $Re \geq 2300$ and approach $Nu_{lam} = 6$ at $Re \leq 2050$, further validating our numerical approach for the elliptical geometry. Figure 3(b) shows the corresponding results for the finned elliptical pipe. Similarly to the circular pipe (Hidman *et al.*, 2026), the alternating fin design triggers an unsteady flow at $1850 < Re < 1950$, giving significantly enhanced heat transfer rates in the intermediate region $1850 < Re < 2300$. At $Re \leq 1850$ and $Re \geq 2300$, the *Nu*-numbers are close to those of the smooth elliptical pipe and in fair agreement with the Meyer *et al.* (2019) and Gnielinski (1975) correlations, as well as the regression model $Nu_{reg}^{ellipse,alternating}$.

The regression models for *Nu* of the finned elliptical and finned circular pipes are given by

$$Nu_{reg}^{ellipse,alternating} = \begin{cases} \sqrt{Nu_{lam}^2 + \left(-0.321\, Re^{0.2} Pr^{0.21}\right)^2} & Re < 1850 \\ \sqrt{Nu_{lam}^2 + \left(1.96\,(Re - 1849.9)^{0.295} Pr^{0.29}\right)^2} & Re \geq 1850 \end{cases} \tag{11}$$

$$Nu_{reg}^{circ,alternating} = \begin{cases} \sqrt{Nu_{lam}^2 + \left(5.5 \times 10^{-7}\, Re^{1.77} Pr^{0.5}\right)^2} & Re \leq 1700 \\ \sqrt{Nu_{lam}^2 + \left(0.86\,(Re - 1699)^{0.39} Pr^{0.32}\right)^2} & Re > 1700 \end{cases} \tag{12}$$

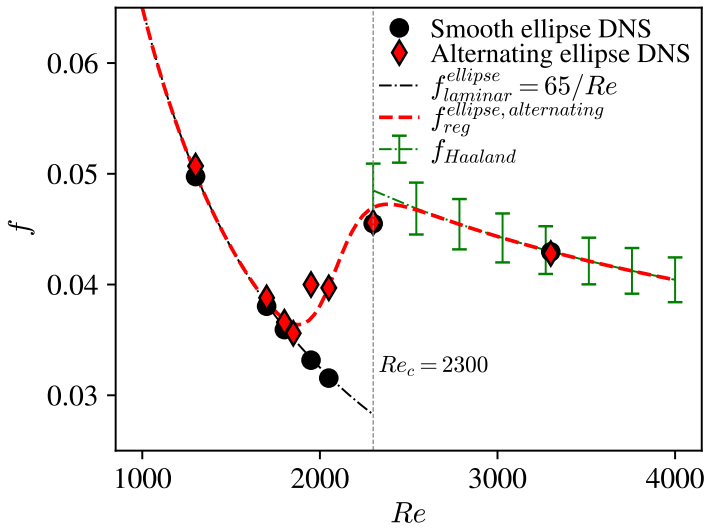

Figure 2: Predicted friction factor for the smooth and finned elliptical pipes together with the laminar solution $f_{laminar}^{ellipse} = 65/Re$, the regression model $f_{reg}^{ellipse,alternating}$ and the Haaland correlation (Haaland, 1983) (±5%). The smooth elliptical pipe shows excellent agreement with the laminar solution at $Re \leq 2050$ and with the Haaland correlation at $Re \geq 2300$. The alternating fin design triggers an earlier transition to unsteady flow at $1850 < Re < 1950$, while maintaining practically the same friction factor as the smooth pipe outside of this region.

It should be noted that $Nu_{lam} = 6$ in (11) and (12) is the theoretical laminar Nusselt number obtained with the uniform cooling term S_Q used in the present DNS. For practical geothermal applications with a constant wall temperature boundary condition, the classical value $Nu_{lam} \approx 3.66$ for circular ducts should be used instead. For the elliptical geometry considered here ($a/D_h = 0.62$, $b/D_h = 0.425$), the laminar Nusselt number under a constant wall temperature boundary condition is expected to be close to 3.66, and we therefore recommend using $Nu_{lam} = 3.66$ in (11) for practical applications. Both models use a square-root blending of the laminar solution with a power-law expression for the effects of the finned geometry. The transition begins at $Re = 1850$ for the elliptical pipe and $Re = 1700$ for the circular pipe, consistent with the DNS results.

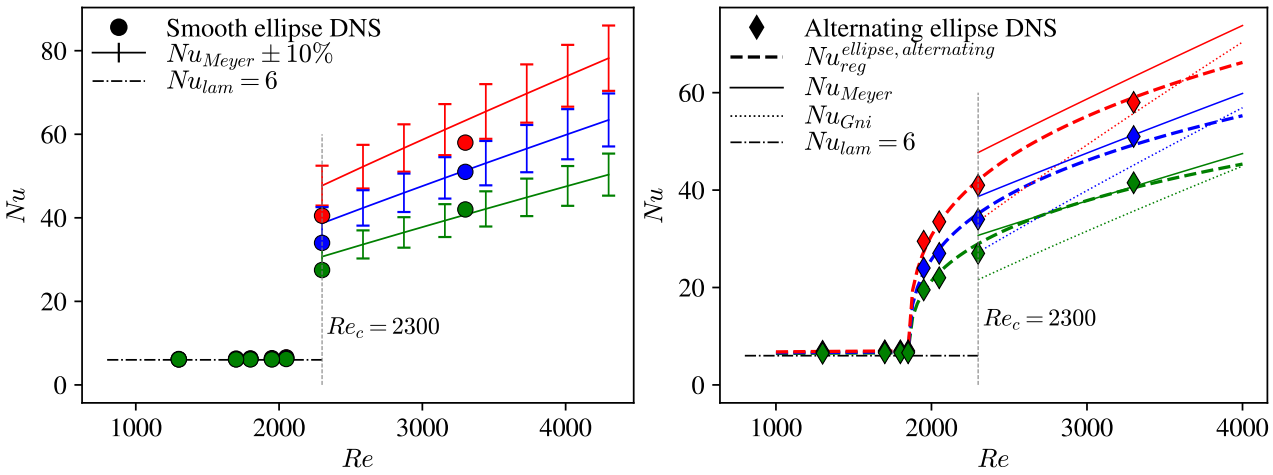

(a) (b)

Figure 3: Predicted Nu-numbers for $Pr = (20, 40, 75)$ (green, blue and red, respectively) and comparison to the laminar solution $Nu_{lam} = 6$ and the correlation of Meyer *et al.* (2019) ($\pm 10\%$). (a): Smooth elliptical pipe DNS. The results are in fair agreement with the Meyer correlation at $Re \geq 2300$ and approach $Nu_{lam} = 6$ at $Re \leq 2050$, validating our numerical approach. (b): Finned elliptical pipe DNS together with the regression model $Nu_{reg}^{ellipse,alternating}$ and the Gnielinski correlation (Gnielinski, 1975). The alternating fin design triggers an unsteady flow at $1850 < Re < 1950$, giving significantly enhanced heat transfer rates compared to the laminar solution in the intermediate region $1850 < Re < 2300$.

3.2 Performance comparison of finned elliptical and finned circular pipes

Figure 4 compares the regression models for the friction factor (7) and (8) and Nu (11) and (12) of the finned elliptical and finned circular pipes. Overall, the two geometries show very similar thermohydraulic performance across the full range of Re. For the friction factor in figure 4(a), both models are in good agreement with the Haaland correlation at $Re \geq 2300$ and deviate from the laminar solution at approximately the same Re, although the transition for the elliptical pipe is shifted slightly towards higher Re (begins at $Re = 1850$) compared to the circular pipe ($Re = 1700$). For the Nu-number in figure 4(b), both models approach $Nu_{lam} = 6$ at low Re and are in fair agreement with the Meyer *et al.* (2019) and Gnielinski (1975) correlations at $Re \geq 2300$. The main difference is again the slightly delayed transition for the elliptical pipe.

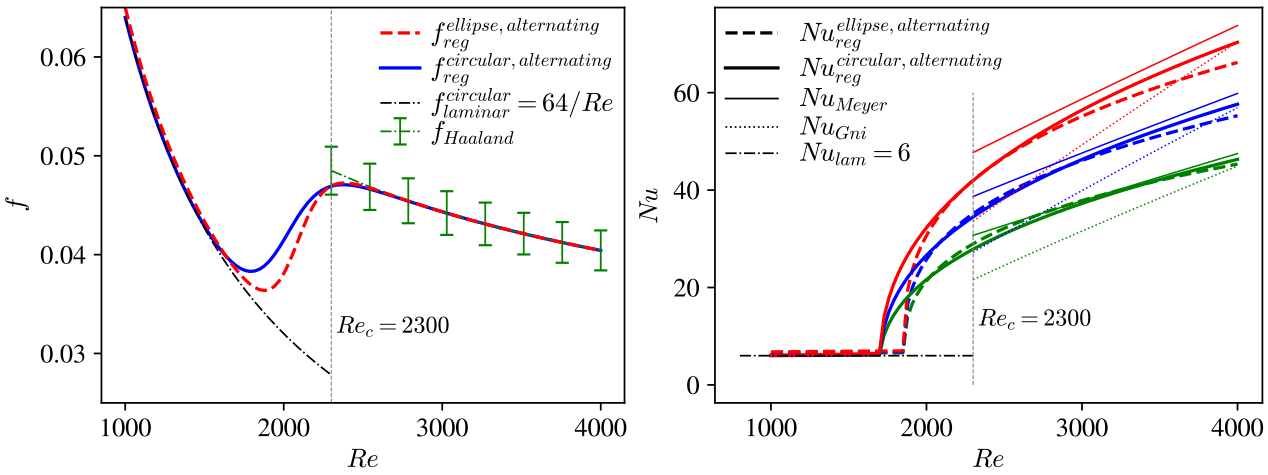

(a) (b)

Figure 4: Comparison of regression models for the finned elliptical and finned circular pipes (7), (8), (11) and (12). (a): Friction factor together with the laminar solution $f_{laminar}^{circular} = 64/Re$ and the Haaland correlation (Haaland, 1983) (±5%). (b): Nu-number for $Pr = (20, 40, 75)$ (green, blue and red, respectively) together with the laminar solution $Nu_{lam} = 6$, the Meyer correlation (**?**) and the Gnielinski correlation (Gnielinski, 1975). The two geometries show similar overall performance, with the main difference being a slightly delayed transition to unsteady flow for the elliptical pipe.

3.2.1 Finned elliptical versus finned circular pipes at equal volumetric flow rate

The regression models derived in section 3.1 are here used to compare the thermohydraulic performance of the finned elliptical and finned circular pipes at the same volumetric flow rate Q. This comparison may be more practically relevant than a comparison at the same Re, since in a real geothermal system the circulation pump delivers a given Q rather than a given Re. The calculations are performed for a 30% ethylene glycol solution with dynamic viscosity $\mu = 4.31 \times 10^{-3}$ Pa·s and density $\rho = 1046$ kg/m^3. The elliptical pipe has outer dimensions 51.5×37 mm with a wall thickness of 2.7 mm, giving inner semi-major and semi-minor axes $a = 23.05$ mm and $b = 15.80$ mm, a cross-sectional area $A = \pi ab = 1144$ mm^2 and hydraulic diameter $D_h = 4A/P = 37.2$ mm. The circular pipe has inner diameter $D = 39.6$ mm and cross-sectional area $A_{circ} = \pi(D/2)^2 = 1232$ mm^2. Note that the elliptical pipe thus has a slightly smaller cross-sectional area than the circular pipe.

For the same Q, the elliptical and circular pipes therefore operate at slightly different Re due to their different cross-sectional areas and hydraulic diameters. Figure 5 shows the Re-number as a function of Q for both geometries, where the elliptical pipe consistently operates at a slightly higher Re than the circular pipe for the same Q, reflecting its smaller cross-sectional area and, consequently, higher flow velocity.

Figure 6(a) shows the friction factor as a function of Q for both pipes. The two geometries show practically the same f across most of the Q-range, with the circular pipe exhibiting a slightly higher f in the transitional region. This is mainly because the circular pipe transitions to unsteady flow at a lower Re ($Re = 1700$) than the elliptical pipe ($Re = 1850$). Figure 6(b) shows the Nu-number as a function of Q for $Pr = (20, 40, 75)$. The two geometries show similar Nu across most of the Q-range, with the circular pipe giving slightly higher Nu in the transitional region for the same reason.

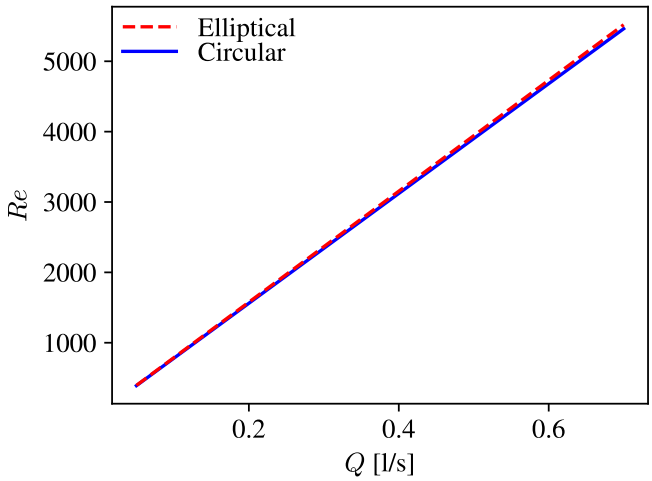

Figure 5: Reynolds number as a function of volumetric flow rate Q for the finned elliptical and finned circular pipes. For the same Q, the elliptical pipe operates at a slightly higher Re due to its smaller cross-sectional area.

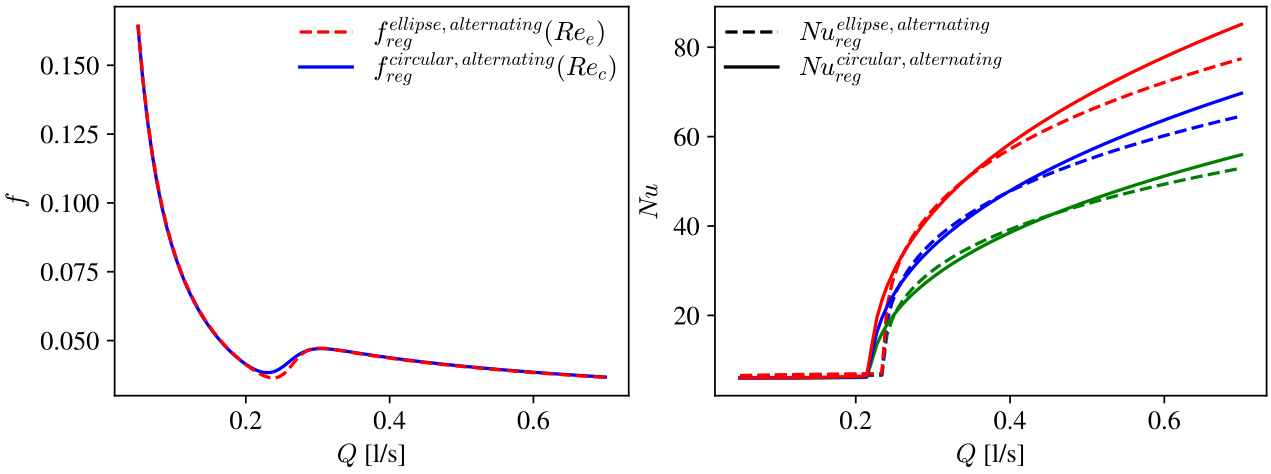

Figure 6: Comparison of the finned elliptical and finned circular pipes at equal volumetric flow rate Q. (a): Friction factor. (b): Nu-number for $Pr = (20, 40, 75)$. Both models are evaluated using the regression models of (7), (8), (11) and (12).

4 Conclusions

We perform fully resolved Direct Numerical Simulations (DNS) of smooth and internally finned elliptical pipes to assess the thermohydraulic performance at conditions relevant for geothermal heating systems ($1300 \leq Re \leq 3300$ and $20 \leq Pr \leq 75$). The fin design follows the promising alternating helical configuration identified in Hidman *et al.* (2026) ($h_{fin} = 0.015D_h$, $n_{fin} = 16$, $\omega_{fin} = 360°$), applied here to an elliptical cross-section with $a/D_h = 0.62$ and $b/D_h = 0.425$.

The smooth elliptical pipe results are validated against the Meyer correlation and the laminar solution, showing good agreement and confirming that $Nu \approx 6$ at low Re with our numerical approach. The alternating helical fin design is shown to trigger an unsteady flow at $1850 < Re < 1950$ for the elliptical pipe, slightly higher than the $1700 < Re < 1800$ observed for the circular pipe in Hidman *et al.* (2026). Outside of this transitional region, the friction factor of the finned elliptical pipe is practically the same as that of the smooth elliptical and smooth circular pipe and in good agreement with the Haaland correlation at $Re \geq 2300$. In the intermediate region $1850 < Re < 2300$, the alternating fin design gives significantly enhanced heat transfer rates of about 300–600% compared to the laminar solution, consistent with the circular pipe results of Hidman *et al.* (2026).

Regression models for the friction factor and Nu-number of the finned elliptical pipe are presented in (7) and (11) and compared to the corresponding models for the finned circular pipe. The two geometries show very similar overall thermohydraulic performance. When compared at the same volumetric flow rate Q, the elliptical pipe operates at a slightly higher Re than the circular pipe due to its smaller cross-sectional area, and both geometries give practically the same f and Nu, with the circular pipe showing slightly higher values in the transitional region.

Overall, the results suggest that the elliptical pipe with alternating helical fins is a promising alternative to the circular finned pipe for geothermal applications. The elliptical geometry offers the additional practical advantages of fitting into a narrower borehole and placing the pipe wall in closer proximity to the borehole wall, potentially reducing the borehole thermal resistance, while delivering thermohydraulic performance comparable to that of the circular finned pipe studied in Hidman *et al.* (2026).

References

Gnielinski, V. 1975 Neue gleichungen für den wärme-und den stoffübergang in turbulent durchströmten rohren und kanälen. *Forschung im Ingenieurwesen A* **41**, 8–16.

Haaland, S.E. 1983 Simple and explicit formulas for the friction factor in turbulent pipe flow. *Journal of Fluids Engineering* **105** (1), 89–90.

Hidman, N., Almgren, D., Johansson, K. & Nilsson, E. 2026 How internal fins enhance the thermohydraulic performance of geothermal pipes: A direct numerical simulation study. *International Journal of Heat and Mass Transfer* **256**, 128114.

Meyer, J.P., Everts, M., Coetzee, N., Grote, K. & Steyn, M. 2019 Heat transfer coefficients of laminar, transitional, quasi-turbulent and turbulent flow in circular tubes. *International Communications in Heat and Mass Transfer* **105**, 84–106.

Pirozzoli, S., Romero, J., Fatica, M., Verzicco, R. & Orlandi, P. 2022 Dns of passive scalars in turbulent pipe flow. *Journal of Fluid Mechanics* **940**, A45.

White, F.M. & Majdalani, J. 2006 *Viscous fluid flow*, , vol. 3. McGraw-Hill New York.